Pergamon

Acta mater. 49 (2001) 1507–1513

Acta MATERIALIA

www.elsevier.com/locate/actamat

MECHANICAL PROPERTIES OF $Zr_{56.2}Ti_{13.8}Nb_{5.0}Cu_{6.9}Ni_{5.6}Be_{12.5}$ DUCTILE PHASE REINFORCED BULK METALLIC GLASS COMPOSITE

F. SZUECS†, C. P. KIM and W. L. JOHNSON

Keck Laboratory of Engineering Materials, California Institute of Technology, Pasadena, CA 91125, USA

(Received 6 October 2000; received in revised form 2 February 2001; accepted 2 February 2001)

Abstract—Ductile phase containing bulk metallic glass composites are prepared via an in situ method by rapid quenching of a homogenous $Zr_{56.2}Ti_{13.8}Nb_{5.0}Cu_{6.9}Ni_{5.6}Be_{12.5}$ melt. The microstructure of the resulting two phase material is investigated by SEM, X-ray diffraction, and microprobe analysis. The composite material, as well as single phase materials with the corresponding matrix and second phase compositions, are tested in uniaxial tension and compression. Young's Modulus, shear modulus and Poisson ratios are analyzed by ultrasonic sound velocity measurements. The composite material demonstrates strongly improved Charpy impact toughness (by a factor of 2.5 compared to Vitreloy 1) and ductility (average fracture strain up to 8.3% in compression and 5.5% in tension). These remarkable improvements are explained by the effect of the mechanically soft and ductile second phase, which acts stabilizing against shear localization and critical crack propagation.

Keywords: Metallic glasses; Composites; Microstructure; Shear bands; Mechanical properties

1. INTRODUCTION

The $Zr_{41.2}Ti_{13.8}Cu_{12.5}Ni_{10}Be_{22.5}$ (Vitreloy 1) bulk metallic glass exhibits an exceptional glass forming ability with a critical cooling rate of ~1 K/s, which makes it a very interesting material for structural applications. This has motivated a series of investigations of its mechanical properties [1–3]. The Vitreloy 1 alloy shows a tensile strength of 1.9 GPa, and an elastic strain limit of 2% under compressive or tensile loading. Plain strain fracture toughness measurements on Vitreloy 1 have revealed values between K_{1C}=18–55 MPa $m^{1/2}$ [3–5], depending on purity and residual stresses of the tested material. However, Vitreloy 1, as all other metallic glasses, fails by the formation of highly localized shear bands, which leads to catastrophic failure under unconstrained conditions without much macroscopic plasticity [1, 2, 6]. This quasi-brittle deformation behavior has limited the application of bulk metallic glasses as an engineering material so far. The preparation of bulk metallic glass matrix composites with ductile metal and refractory ceramic particles as reinforcements has yielded improvements in tensile and compressive strains to failure [7–9]. Multiple shear bands are observed when the catastrophic instability is avoided by mechanical constrains. In this paper we present a new ductile metal reinforced bulk metallic glass material prepared via a cost effective in situ processing method [10, 11]. This composite exhibits large compressive and tensile strains to failure and a strongly improved impact toughness compared to other metallic glass materials.

2. EXPERIMENTAL

Cu (99.999%), Ni (99.995%), and Ti (99.995%) from Cerac, Inc., Nb (99.8%) from Alfa Aesar, crystal bar Zr with less than 300 ppm oxygen content from Teledyne Wah-Chang Inc., and Be (99.99%) from Electronic Space Products International were used as raw materials for arc melting. Four different alloy compositions were prepared in the form of 25 g rods by plasma arc melting in a Ti-gettered argon atmosphere on a water cooled copper plate. The best homogeneity of the final melt was reached after a four step melting procedure: first, elemental Nb and Zr was melted together, followed by the addition of Be. Then elemental Cu, Ni and Ti were melted together in a second batch and finally both ingots were melted together and remelted several times until a homogenous melt was formed. From our experience with the arc melting setup the water cooled copper plate provides a cooling rate of approximately 1–100 K/s in

† To whom all correspondence should be addressed. Haesingerstr. 34, 4055 Basel, Switzerland.

E-mail address: szuecs@caltech.edu (F. Szuecs)

1359-6454/01/$20.00
PII: S1359-6454(01)00068-4

the critical temperature range between T_g and T_l after turning the arc off. The temperature field under the arc has a steep gradient towards the copper plate because of which the actual temperatures and cooling rates could not be determined experimentally.

In addition, commercially cast (Howmet, Inc.) 3.3 mm thick plates, labeled as material H, with same composition as for alloy C were used. Table 1 gives the compositions and phases of the investigated materials. Scanning electron microscopy (SEM) was used for the analysis of the as-cast microstructures and fracture surfaces using a Camscan Series II. The chemical compositions were determined using a JOEL JXA-73 electron microprobe analyzer with elements of Zr, Ti, Nb, Cu and Ni as standards; whereas the Be content was calculated by difference. The structures of the reinforcing phase and the interface were analyzed with a Philips EM430 transmission electron microscope (TEM). X-ray diffraction patterns were obtained with an INEL diffractometer using Co K_α radiation ($\lambda = 0.179$ nm), as a CPS-120 position sensitive detector and Si as an internal standard.

Ultrasonic sound velocity measurements were performed to obtain room-temperature Young's modulus, shear modulus and Poisson ratios of the specimens using the standard procedure of this method and measuring mass densities according to the Archimedes principle. Sub-standard sized Charpy specimens with 5×5 mm cross section and 1 mm V-notch depth were prepared and tested on an usual Charpy impact testing machine. An Instron 4202 load frame was used to test two or three specimens of each type at room-temperature under uniaxial compression and tensile loading. The compression test specimens were 6 mm in length, either cylindrical with 3 mm diameter or rectangular with a 3×3 mm^2 cross section and polished plan parallel to an accuracy of less than 10 μm. The compression samples were sandwiched between two WC platens in a loading fixture designed to guarantee axial loading. The ends of the compression samples were lubricated to prevent 'barreling' of the sample. The tensile test specimens were machined into a dog-bone geometry with dimensions proportional to ASTM standard E8-68. Strain gages (Micromeasurement Group) glued on the surface of the specimen's gage section were used to obtain one-dimensional surface strains. All compression and tensile tests were conducted using constant strain rates between 10^{-6} and 10^{-4} s^{-1}.

3. RESULTS AND DISCUSSION

3.1. Microstructures

All investigated compositions are shown in Table 1 together with a summary of X-ray diffraction and ultrasonic sound velocity measurement results. All compositions lie on one line of a pseudo-ternary phase diagram with apexes of zirconium, (titanium+niobium), and X, where X represents the moiety $Cu_5Ni_4Be_9$, as shown in Fig. 1. This line can also be written as $(Zr_{75}Ti_{25-x}Nb_x)_{100-y}X_y$. Vitreloy 1, the best glass former known so far in the Nb-free Zr–Ti–Cu–Ni–Be system, with a composition of $Zr_{41.2}Ti_{13.8}Cu_{12.5}$ $Ni_{10}Be_{22.5}$ lies on the same line ($x = 0$, $y = 45$) within the bulk metallic glass forming compositional region shown as a circle in Fig. 1.

Samples with starting compositions M and B yield single phase materials. Composition M is a bulk metallic glass former whereas composition B yields a fully crystalline material with grain sizes about ~100 μm. Material B has a body-centered cubic (bcc) or β phase structure, as investigated by SEM and X-ray analysis.

Figure 2 shows the backscattering SEM images of a polished and chemically etched cross section of composite materials C and H. The composition of these samples lies in the two phase region between M and B. Upon cooling, the homogenous melt chemically partitions into approximately 25 vol% of a den-

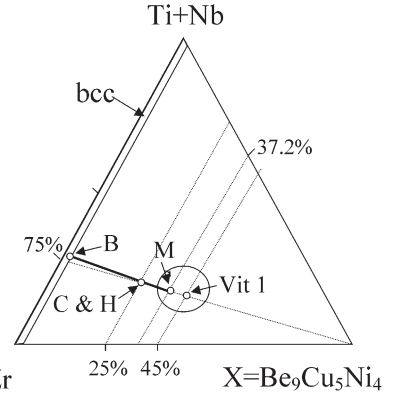

Fig. 1. Pseudo-ternary phase diagram with the apexes of Zr, (Ti+Nb) and ($Be_9Cu_5Ni_4$). Compositions of Vitreloy 1, single phase materials M and B, and composites C and H are marked. A circle indicates the compositional region, within monolithic bulk metallic glasses can be obtained with copper mold casting techniques.

Table 1. Phases analyzed by X-ray diffraction (bcc: body centered cubic; bmg: bulk metallic glass), mass densities by the Archimedes method, Young's modulus, shear modulus and Poisson ratios resulting from ultrasonic sound velocity measurements for samples with given chemical compositions. Materials C, M and B were prepared at Caltech, H and Vitreloy 1 at Howmet, Inc

Sample	Composition	Phases	δ (g cm^{-3})	E (GPa)	G (GPa)	ν
Vitreloy 1	$Zr_{41.2}Ti_{13.8}Cu_{12.5}$ $Ni_{10}Be_{22.5}$	bmg	6.1	97.2	35.9	0.355
C and H	$Zr_{56.2}Ti_{13.8}Nb_{5.0}Cu_{6.9}Ni_{5.6}Be_{12.5}$	bmg+bcc	6.2	78.8	28.6	0.375
M	$Zr_{47}Ti_{12.9}Nb_{2.8}Cu_{11}Ni_{9.6}Be_{16.7}$	bmg	6.3	89.2	32.6	0.369
B	$Zr_{71}Ti_{16.3}Nb_{10}Cu_{1.8}Ni_{0.9}$	bcc	6.5	63.3	22.7	0.401

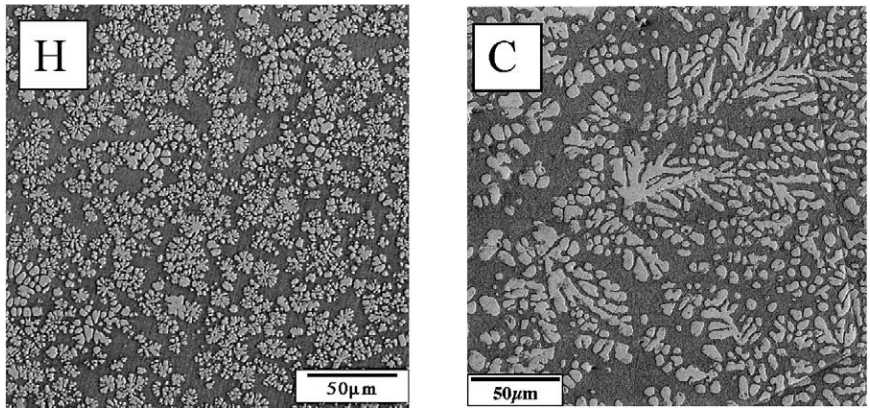

Fig. 2. Backscattering SEM images of polished and chemically etched cross sections of composites C and H. The β phase dendrites appear bright, the fully amorphous matrix phase appears dark. A mixture of diluted fluoric and phosphoric acid was used as etchant.

dritic bcc phase with the same composition as sample B, which is embedded into the remaining fully amorphous matrix phase of same composition as sample M, according to electron probe chemical analysis. The dendritic structure is characterized by primary dendrite axes with lengths of 50–150 µm and a radius of 1.5–2 µm. Regular patterns of secondary dendrite arms with spacings of 6–7 µm are observed. For the commercially cast material H, which was probably processed with a slightly higher cooling rate (not determined experimentally), a finer dendritic structure than for material C was found. X-ray diffraction shows no crystalline phases other than that of the monolithic bcc sample B (Fig. 3).

We believe that on cooling from the high-temperature melt, the alloy undergoes partial crystallization by nucleation and subsequent dendritic growth of the β phase in the remaining liquid. The remaining liquid, after cooling below its glass transition temperature (considered as a solidus) freezes to the amorphous or glassy state, producing a two-phase microstructure containing β phase dendrites in a bulk metallic glass matrix. Depending on the cooling rate coarser or finer dendritic structures can be obtained. The compositions within the two phases do not vary locally within the experimental error of electron probe analysis. This implies solute redistribution and the establishment of chemical equilibrium within and between the phases following dendritic growth.

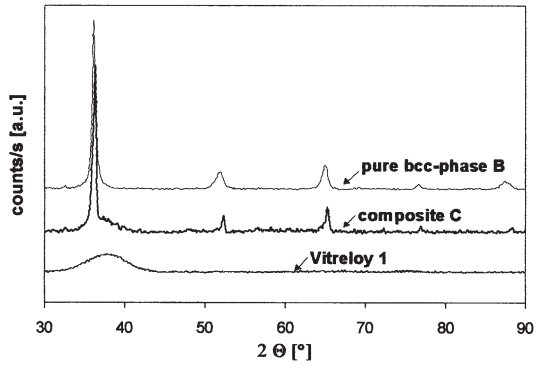

Fig. 3. X-ray diffraction pattern of Vitreloy 1, monolithic bcc sample B, and composite C.

3.2. Mechanical properties

A series of mechanical tests were conducted on samples C, H, M, B and Vitreloy 1. Figure 4 shows uniaxial compressive stress–strain curves typical for the composite material H and the single phase materials M and B. Figure 5 shows typical tension test results for Vitreloy 1, composites C and H. All test results are summarized in Table 2.

Under quasi-static compressive loading all materials exhibit a Young's modulus very close to the results measured with the ultrasonic sound method (Table 1). Ultrasonic Young's moduli decrease from 97.2 GPa for Vitreloy 1 to 89.2 GPa for the monolithic matrix composition M and to 78.8 GPa for the composite sample C. For the monolithic β phase sample B the drop in Young's modulus (63.3 GPa) is even more pronounced and especially the shear modulus of 22.7 GPa reaches a very low value. This indicates that the β phase structure is unstable against shear. For the metallic glass containing materials Vitreloy 1, C, and H the Young's moduli determined from the tensile stress–strain curves are constantly ~10% lower compared to results from compression testing and ultrasonic sound measurements, which is not well understood yet and has to be verified. We think that the differences in the elastic modulus can possibly be explained by a mean stress dependence of the elastic behavior for metallic glasses.

The monolithic bulk metallic glass materials (samples Vitreloy 1 and M) show linear elastic behavior up to yield stresses of ~1600–1750 MPa in compression and fracture stresses of 1500–1750 MPa in tension. They fail being quasi-brittle without any macroscopic plasticity at fracture strains below 2% in tension and show only minor plasticity up to fracture strains of ~3.3% in compression. Compared to Vitre-

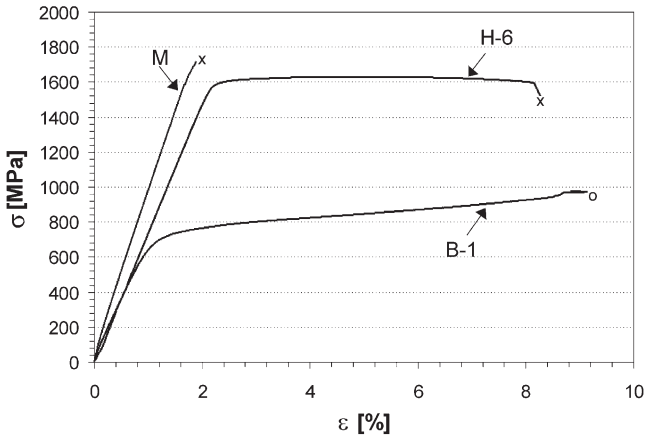

Fig. 4. Uniaxial stress strain curves in compression for single phase materials M and B and for composite H. Symbols ×: fracture; ○: the test run on specimen B-1 was stopped without fracture of the sample, because it was losing its cylindrical shape.

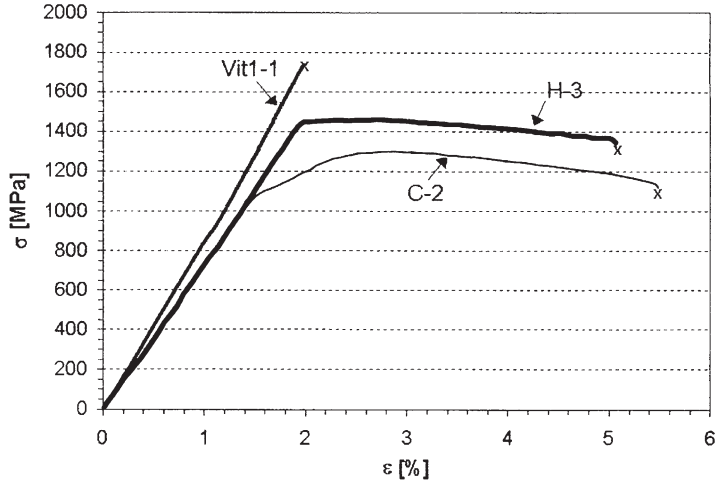

Fig. 5. Uniaxial stress strain curves in tension for Vitreloy 1 and the two composite materials C and H. Symbol ×: fracture.

Table 2. Summary of tensile and compressive test data. Samples of C, M and B were prepared at Caltech, Vitreloy 1 (vit1) and composite H were cast at Howmet, Inc. Young's modulus E, yield stress σ_y, strain at the yield point ϵ_y, ultimate strength σ_{max} and strain at ultimate stress $\epsilon_{@max}$, as well as fracture strain ϵ_f are listed. For samples with pronounced plasticity the average strain rate in the plastic region $(d\epsilon/dt)_{pl}$ is given as well. Test runs on samples H-4, B-1 and B-2 were stopped without reaching fracture

	Sample	E	σ_y (GPa)	ϵ_y (MPa)	σ_{max} (%)	$\epsilon_{@max}$ (%)	ϵ_f (%)	$(d\epsilon/dt)_{pl}$ (s^{-1})
Tension	vit1-1	86.9	–	–	1737	1.98	1.98	–
	vit1-2	88.4	–	–	1571	1.80	1.80	–
	vit1-3	84.3	–	–	1525	1.80	1.80	–
	H-1	71.4	1450	2.07	1486	3.03	4.54	9.4×10^{-5}
	H-2	72.6	1420	1.97	1487	2.93	4.85	8.0×10^{-6}
	H-3	74.2	1410	1.90	1465	2.57	5.07	9.3×10^{-5}
	C-1	71.1	1114	1.58	1296	2.64	4.74	8.8×10^{-5}
	C-2	72.7	1100	1.53	1327	2.82	5.00	8.8×10^{-5}
	C-3	72.4	1064	1.48	1302	2.70	5.49	1.0×10^{-4}
compression	vit1-4	96.3	1637	1.83	1755	2.09	2.09	–
	vit1-5	98.4	1742	1.76	1899	3.33	3.33	3.2×10^{-5}
	H-4	80.1	1545	1.90	1669	4.70	Stopped	–
	H-5	78.4	1520	1.97	1646	4.04	6.32	1.3×10^{-4}
	H-6	75.0	1480	2.02	1628	5.90	8.26	9.5×10^{-5}
	M-1	92.5	1588	1.67	1715	1.89	1.89	–
	M-2	84.0	1593	1.60	1644	1.66	1.66	–
	B-1	65.2	550	0.80		Stopped at ϵ ~9%		1.7×10^{-4}
	B-2	60.5	540	0.87	1006	13.4	Stopped	5.2×10^{-4}

loy 1 the matrix sample M has slightly degraded mechanical properties with a lower Young's modulus, yield and fracture stress and lower fracture strains.

Much higher average fracture strains of ~8% in compression and ~5% in tension were reached for the composite samples C and H. The yield stresses are between ~1100 MPa (sample C in tension) and ~1500 MPa (sample H in compression), depending on the loading direction and microstructural features, e.g. the average dendrite arm spacing of the β phase. The yield stresses in compression are constantly higher than in tension, which again indicates a mean stress sensitivity of the bulk metallic glass containing materials. The yield criterion in metallic glasses has not been unambiguously established so far. Bruck et al. [1] have established that there is no difference between compressive and tensile yield strengths and concluded a von Mises yield criterion, whereas Donovan [12] investigated a Pd glass and concluded that it follows a Mohr–Coloumb yield criterion. Our results confirm that the investigated bulk metallic glass materials do not follow a von Mises yield criterion, as proposed by Bruck.

A work hardening behavior is observed for the all test runs on composite samples. An ultimate strength up to ~1670 MPa is reached in compression and ~1490 MPa in tension. Tensile specimens show clear necking with plastic strains up to 15% at the necked region. In the range of applied strain rates no significant strain rate sensitivity is detectable. In addition, dramatic improvements in impact toughness compared to monolithic Vitreloy 1 are found. The composite material C shows sub-standard sized Charpy V-notch impact resistance of 20.0 J, which is higher by a factor of 2.5 than the test result for Vitreloy 1 (8.0 J). The composite fracture surfaces show a mixed fracture mode of II and III with distinct shear lips near the edges of the specimen under the dynamic loading condition of the Charpy test. The average value of the angle between the slip plane and the loading axis was 45°. The higher energy absorption during fracture can be explained by the increased plastic strain to failure.

Measurements on the monolithic β phase material B show high ductility. The yield stress is only 540–550 MPa. After extended work hardening an ultimate strength of ~1000 MPa at a strain of ~13% is measured. The compressive test runs were stopped at total strains of 9 and 21% without reaching fracture, because the test specimen were losing their cylindrical shape. A unique feature of the stress–strain data was observed for material B in the plastic region: the stress values plotted over time show slight sinusoidal fluctuation of the yield stress with ongoing plastic deformation (Fig. 6), which is clearly a material specific behavior and not caused externally. Such a behavior is commonly called serrated flow, but it clearly differs from the serrated flow observed in bulk metallic glasses, which is characterized in sudden load drops at each progression of a slip band (Fig. 7).

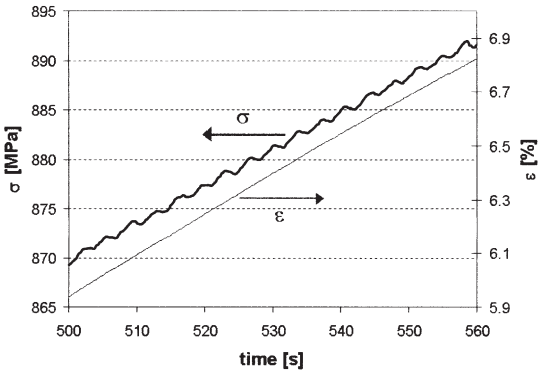

Fig. 6. Compressive stress and strain data of the plastic region plotted over time for the monolithic β phase sample B-1. Work hardening behavior with fluctuations in the yield stress is observed with ongoing plastic deformation.

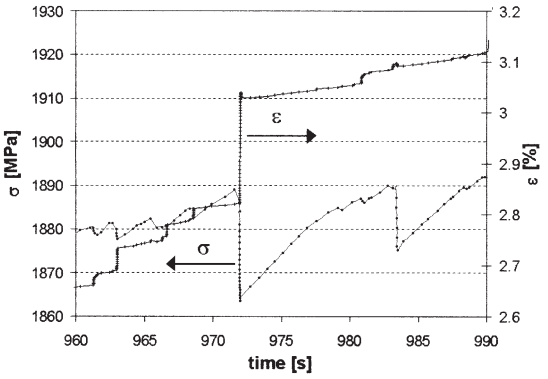

Fig. 7. Compressive stress and strain data of the plastic region plotted over time for the vit1-5 bulk metallic glass sample. Serrated flow behavior with sudden stress drops during single slip events is observed.

The composite materials H and C also show similar yield stress fluctuations with ongoing deformation as material B, but at much higher stress levels (Fig. 8).

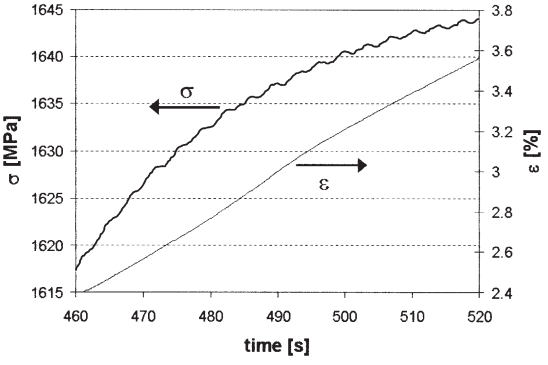

Fig. 8. Compressive stress and strain data of the plastic region plotted over time for composite sample H-5. Same fluctuations in yield stress as for material B is observed, but at much higher stress values.

3.3. Deformation, fracture and toughening mechanism

An SEM analysis of plastically deformed regions and of fracture surfaces show significant differences for the composite materials compared to monolithic bulk metallic glasses. As shown in Fig. 9 the fracture surfaces are still oriented under a global 45° angle to the loading axis. However, at higher magnifications (Fig. 9, inset) we see that the fracture surface of the composite is more complex showing some regions with vein patterns, as also seen for Vitreloy 1, together with other large regions with higher roughness, which also appear to have undergone extensive melting and resolidification showing evidence for enormous heat dissipation during surface separation. The side view on a prior-to-testing mirror polished surface of a tensile specimen shows increasingly dense patterns of multiple shear bands as we come closer to the fracture surface (Fig. 10). Necking of the gauge section over several millimeters length is also clearly visible.

Dislocation motion, twinning and phase transformation induced plasticity are possible mechanisms of plasticity of the β phase. Based on the initial TEM analysis we found evidence for the existence of twins and/or martensitic phase boundaries in the β phase dendrites. The low shear modulus and the serrated flow behavior also suggest that twinning and phase transformations contribute to plastic deformation of the β phase. The composition of the β phase is very close to the α–β phase boundary in the Zr–Ti–Nb system, which also indicates a possible instability of the β phase for phase transformations. In contrast to the dislocation motion and shear banding, twinning and phase transformations are mechanisms with *limited* plastic strain for each local event. Further plastic deformation must proceed at a different location at higher stresses. This explanation could lead to the observed serrated flow behavior of the β phase.

We propose that upon yielding of the composite the soft β phase dendrites deform first. Simultaneously load is transferred to the surrounding glass matrix, causing nucleation of a shear band. Upon further loading the nucleated shear band propagates and interacts with other dendrite arms and/or shear bands. Nevertheless, the propagation of single shear bands seems to be restricted, possibly by a limiting local plastic strain mechanism described above. This hinders a single shear band to extend critically through the whole sample at the onset of plastic deformation and cause early fracture. Instead plasticity is distributed more homogeneously in the form of shear band patterns, which result in high strains to failure and an apparent work hardening behavior of the composite.

4. CONCLUSIONS

A new class of ductile β phase reinforced bulk metallic glass composites were made by an easily feasible in situ processing method from a homogeneous $Zr_{56.2}Ti_{13.8}Nb_{5.0}Cu_{6.9}Ni_{5.6}Be_{12.5}$ melt. The microstructure of the resulting two phase material consists of a dendritic Zr–Ti rich β phase with a body centered cubic structure, which is embedded in a fully amorphous matrix. Both phases are in chemical equilibrium and show atomically sharp, intimate and apparently strong interfaces. The matrix phase has a very similar composition to Vitreloy 1 and exhibit in monolithic form mechanical properties typical for a bulk metallic glass. The reinforcing β phase shows in monolithic form a soft and ductile mechanical behavior with pronounced work hardening and a serrated flow behavior. Both phases combined in one material yield in a composite with excellent mechanical properties. Compared to Vitreloy 1, the best bulk metallic glass former known so far in the Zr-based system, impact toughness values improved by a factor of 2.5 and

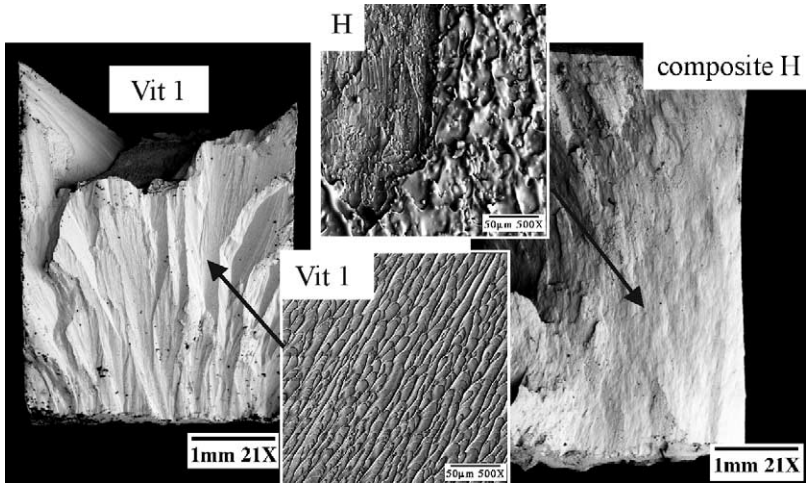

Fig. 9. Backscattering SEM images of fracture surfaces after compression tests on BMG sample Vit1-4 and composite sample H-4.

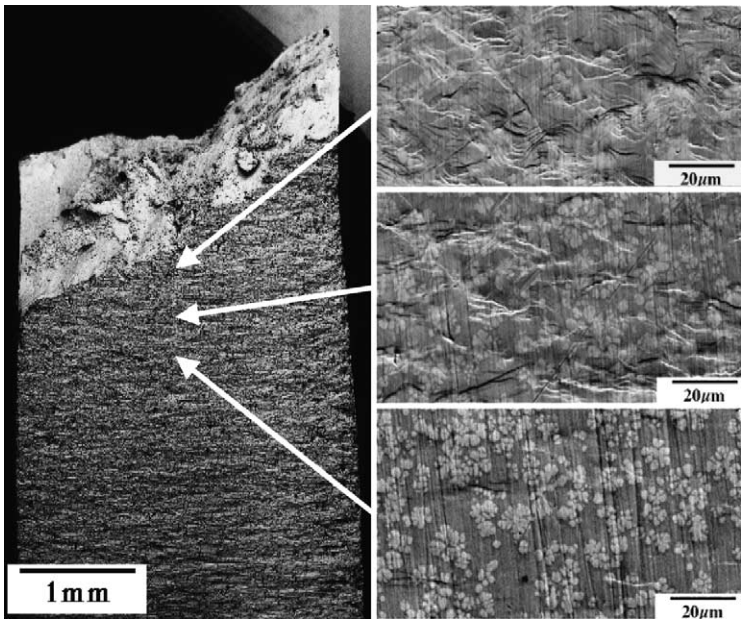

Fig. 10. Backscattering SEM images of the tensile specimen H-2 show a side view of the necking along the gauge section. The density of shear bands decrease with increasing distance from the fracture surface (at 20 μm, 600 μm and 1 mm distance) as visible at higher magnification.

average tensile strains to failure by a factor of 2.7. The yield point and work hardening behavior of the composites can be tailored by the processing conditions. An ultimate tensile strength up to ~1500 MPa was reached. The enhanced plasticity and toughening of the composites can be explained in terms of the deformation mechanism which is dominated by the β phase dendrites.

Acknowledgements—The authors would like to acknowledge the financial support of the US Department of Energy (Grant No. DEFG-03-86ER45242) and the German Science Foundation (Grant Sz 87/1-1).

REFERENCES

1. Bruck, H. A., Christman, T., Rosakis, A. J. and Johnson, W. L., *Scripta Metallurgica Et Materialia*, 1994, **30**(4), 429.
2. Bruck, H. A., Rosakis, A. J. and Johnson, W. L., *Journal of Materials Research*, 1996, **11**(2), 503.
3. Gilbert, C. J., Ritchie, R. O. and Johnson, W. L., *Applied Physics Letters*, 1997, **71**(4), 476.
4. Conner, R. D., Rosakis, A. J., Johnson, W. L. and Owen, D. M., *Scripta Materialia*, 1997, **37**(9), 1373.
5. Lowhaphandu, P. and Lewandowski, J. J., *Scripta Materialia*, 1998, **38**(12), 1811.
6. Alpas, A. T. and Embury, J. D., *Scripta Metallurgica*, 1988, **22**(2), 265.
7. Choi-Yim, H. and Johnson, W. L., *Applied Physics Letters*, 1997, **71**(26), 3808.
8. Conner, R. D., Dandliker, R. B. and Johnson, W. L., *Acta Materialia*, 1998, **46**(17), 6089.
9. Choi-Yim, H., Busch, R., Koster, U. and Johnson, W. L., *Acta Materialia*, 1999, **47**(8), 2455.
10. Hays, C. C., Kim, C. P. and Johnson, W. L., *Physical Review Letters*, 2000, **84**(13), 2901.
11. Kim, C. P., Szuecs, F. and Johnson, W. L., Journal of Metastable and Nanocrystalline Materials, 2001, **10**, 49–54.
12. Donovan, *Acta Metallurgica*, 1989, **37**(2), 445.